



Developing and understanding Leaching-Resistant cobalt nanoparticles via N/P incorporation for liquid phase hydroformylation

Carmen Galdeano-Ruano^a, Silvia Gutiérrez-Tarriño^a, Christian W. Lopes^b, Jaime Mazarío^c, Lidia E. Chinchilla^d, Giovanni Agostini^e, Jose J. Calvino^{d,f}, Juan P. Holgado^g, Enrique Rodríguez-Castellón^h, Alberto Roldanⁱ, Pascual Oña-Burgos^{a,*}

^a Instituto de Tecnología Química, Universitat Politècnica de València-Consejo Superior de Investigaciones Científicas (UPV-CSIC), Avda. de los Naranjos s/n, 46022 Valencia, Spain

^b Department of Chemistry, Federal University of Paraná (UFPR), Curitiba 81531-990, Brazil

^c LPCNO (Laboratoire de Physique et Chimie des Nano-Objets), Université de Toulouse, CNRS, INSA, UPS, 31077 Toulouse, France

^d División de Microscopía Electrónica de los Servicios Centralizados de Investigación Científica y Tecnológica de la Universidad de Cádiz (DME-UCA), Facultad de Ciencias, Universidad de Cádiz, Campus Río San Pedro S/N, Puerto Real 11510, Cádiz, Spain

^e ALBA Synchrotron Light Facility, Carrer de la Llum 2-26, Cerdanyola del Valles, Barcelona 08290, Spain

^f Departamento de Ciencia de los Materiales e Ingeniería Metalúrgica y Química Inorgánica, Facultad de Ciencias, Universidad de Cádiz, Campus Río San Pedro S/N, Puerto Real 11510, Cádiz, Spain

^g Instituto de Ciencia de Materiales de Sevilla and Departamento de Química Inorgánica, CSIC-Universidad de Sevilla, Av. Américo Vespucio, 49, 41092 Seville, Spain

^h Universidad de Málaga, Facultad de Ciencias, Departamento de Química Inorgánica, 29071 Málaga, Spain

ⁱ Cardiff Catalysis Institute, School of Chemistry, Cardiff University, Main Building, Park Place, CF10 3AT, Cardiff, United Kingdom

ARTICLE INFO

Keywords:

Alkene hydroformylation
Cobalt catalysts
Atomistic modelling
N-doped carbon
Heteroatom influence

ABSTRACT

The ultimate target in heterogeneous catalysis is the achievement of robust, resilient and highly efficient materials capable of resisting industrial reaction conditions. Pursuing that goal in liquid-phase hydroformylation poses a unique challenge due to carbon monoxide-induced metal carbonyl species formation, which is directly related to the formation of active homogeneous catalysts by metal leaching. Herein, supported heteroatom-incorporated (P and N) Co nanoparticles were developed to enhance the resistance compared with bare Co nanoparticles. The samples underwent characterization using operando XPS, XAS and HR electron microscopy. Overall, P- and N-doped catalysts increased reusability and suppressed leaching. Among the studied catalysts, the one with N as a dopant, CoN_x@NC, presents excellent catalytic results for a Co-based catalyst, with a 94% conversion and a selectivity to aldehydes of 80% in only 7.5 h. Even under milder conditions, this catalyst outperformed existing benchmarks in Turnover Numbers (TON) and productivity. In addition, computational simulations provided atomistic insights, shedding light on the remarkable resistance of small Co clusters interacting with N-doped carbon patches.

1. Introduction

Hydroformylation transforms olefins and syngas into aldehydes, a crucial feedstock for alcohol, amine, and ester manufacture. These compounds, in turn, are essential for producing polymers, surfactants, and plasticizers [1–4]. The current production of 12 million tons underscores the immense significance of this process [5–8].

The hydroformylation process is industrially executed using homogenous catalysts based on cobalt or rhodium complexes, [9,10]

primarily because cobalt heterogeneous catalysts present leaching issues [11–14]. Cobalt carbonyl species are formed under reaction conditions and detach (leach) from the solid phase (supported material) into the solution. Thus, mitigating metal leaching is of paramount importance as it adversely impacts the catalyst's performance and durability. Furthermore, these cobalt carbonyl species can form deposits on reactor surfaces and clog valves [15]. Regarding environmental issues, cobalt is a recognised pollutant in water that can lead to serious health problems in humans, hence the concern about its releasing [16,17]. Fujimoto *et al.*

* Corresponding author at: Instituto de Tecnología Química, Universitat Politècnica de València-Consejo Superior de Investigaciones Científicas (UPV-CSIC), Avda. de los Naranjos s/n, 46022 Valencia, Spain.

E-mail address: pasoabur@itq.upv.es (P. Oña-Burgos).

<https://doi.org/10.1016/j.jcat.2024.115374>

Received 4 January 2024; Received in revised form 13 February 2024; Accepted 15 February 2024

Available online 24 February 2024

0021-9517/© 2024 The Author(s). Published by Elsevier Inc. This is an open access article under the CC BY-NC license (<http://creativecommons.org/licenses/by-nc/4.0/>).

pioneered the research of leaching in solid catalysts for hydroformylation and reported a pressure-dependent decrease in Co loading of 20 % at 3.0 MPa and 50 % at 5.0 MPa [18]. Recently, Beller, Wen and Hou groups have carefully addressed the problem with cobalt leaching in hydroformylation [19–21]. The former studied the effect of the support and N-containing precursors (ligands with 1 or 2 nitrogen atoms: chitosan, tryptophan, and phenanthroline) on a comprehensive library of catalysts. They concluded that both the precursor and the support influence metal leaching and that more profound research on the topic is still needed [19]. Wen *et al.* found that protectants like formic acid, oxalic acid or citric acid can compete with CO and block Co leaching, but at the expense of catalytic activity, since total suppression of 34.5 % Co leaching led to a drop-off in conversion from 61.0 % to 22.1 % [20]. They also claimed that CoGa alloys can also decrease Co leaching in hydroformylation [22]. Finally, Hou *et al.* demonstrated that the incorporation of phosphorus helps to stabilize cobalt single atoms in ZrP-supported Co materials. In this regard, a recent review from Pan *et al.* indicated that many studies have shown that Co-based catalysts suffer from low activity and poor cycling stability, highlighting the importance of exploring new robust cobalt heterogeneous catalysts for this reaction [23].

Interestingly, combining the use of metal complexes as particle precursors and N-doped carbons has been shown to be beneficial for stabilizing and distributing carbon-supported cobalt-based nanoparticles applied in the reduction of nitro compounds [24–26]. In particular, our recent work demonstrated that the precursor [Co(tpy)₂](NO₃)₂, where Co is coordinated to six nitrogen atoms, leads to the formation of N-doped graphitic carbon layers around metallic nanoparticles [27]. This structural feature is particularly appealing due to the high stability of these carbonaceous materials, offering a potential solution to mitigate intrinsic leaching problems in hydroformylation processes.

On the other hand, the phosphine cobalt catalytic system, HCo(CO)₃(PR₃)₃, has been used industrially as an alternative to HCo(CO)₄, to carry out hydroformylation reactions at lower pressures [9,28]. However, the introduction of phosphorus in cobalt-based heterogeneous catalysts remains largely unexplored. In fact, only two studies approaching the hydroformylation of olefins promoted by catalytic systems with both P and

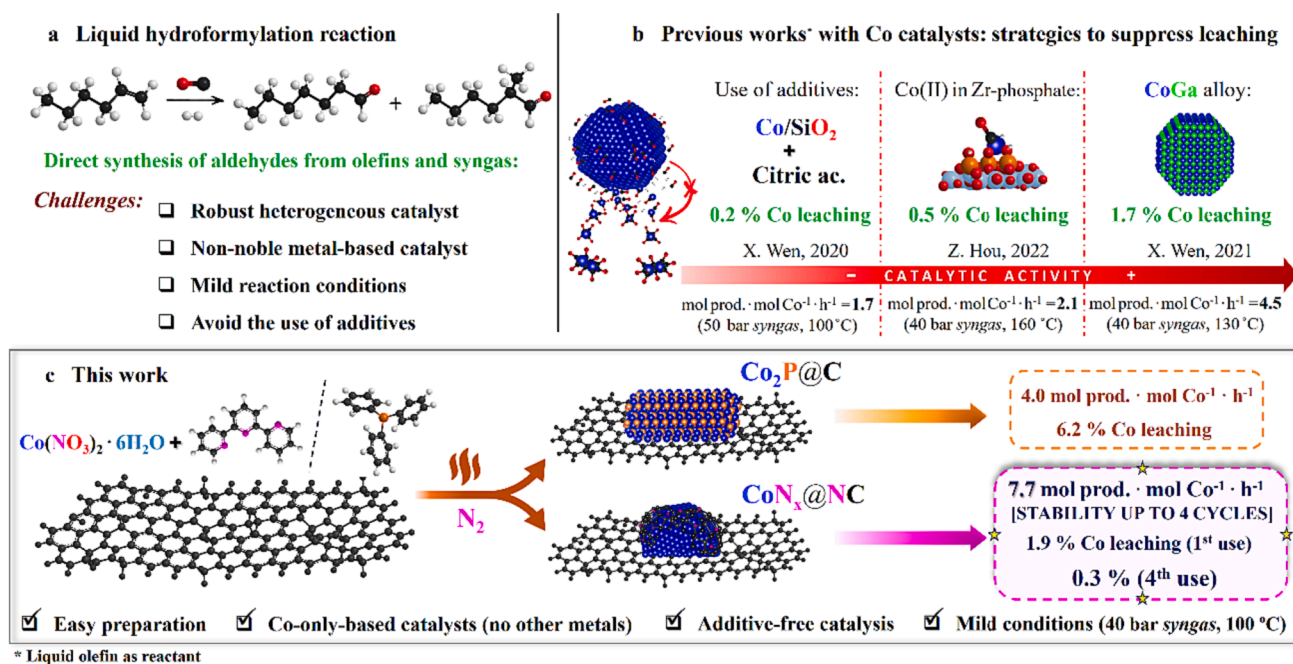
Co have been reported. In one study, they show that cobalt acts as dopant in Rh phosphide species, while in the other, phosphorus was integrated into a zirconium phosphate support [21,29]. Interestingly, unlike cobalt, whose pure phosphide species have never been used in hydroformylation, rhodium phosphide nanoparticles have proved their superiority over those of metallic rhodium in this process [30] (Scheme 1).

In this work, we investigate the utility of N and P heteroatom-containing ligands as precursors for synthesizing durable carbon-supported cobalt nanoparticles. The resulting materials have been thoroughly characterized using HRTEM/STEM, XPS, XAS studies, and isotopic exchange tests, with a focus on their leaching during the catalysis of 1-hexene hydroformylation. All synthesized catalysts have been systematically compared with bare Co nanoparticles, exhibiting significant leaching mitigation and oxidation resistance, affirming their enhanced durability. Notably, among the ligands used, terpyridine formed protective carbon layers around the particles, effectively preventing Co leaching without significantly compromising catalytic activity. Furthermore, the application of PPh₃ as a ligand has led to the development of Co phosphide species which, to the best of our knowledge, constitutes a novel addition to this reaction. The insights underpinning the leaching phenomenon have been rationalized using atomistic simulations based on the Density Functional Theory.

2. Results and discussion

2.1. Synthesis of catalysts

The synthesis procedure aimed to create different cobalt-based materials, including CoN_x@NC, Co₂P@C, Co₂PN_x@NC, and Co@C. Cobalt (II) nitrate hexahydrate always served as the cobalt source, and specific ligands (2,2':6',2''-terpyridine for CoN_x@NC; triphenylphosphine for Co₂P@C and mixture for Co₂PN_x@NC) were added or omitted in varying ratios. The process involves initial stirring of cobalt compounds and ligands in ethanol, then adding carbon powder (VULCAN® XC72R) and overnight stirring. After ethanol removal, the solid is dried, grinded, and subjected to pyrolysis at 800 °C under N₂, with subsequent cooling. Complete details for the synthesis can be found in the ESI.



Scheme 1. Overview of strategies to suppress leaching in liquid-phase hydroformylation using heterogeneous cobalt catalysts and comparative analysis with this work.

2.2. Characterization of catalysts

All catalysts synthesized in this work were exhaustively characterized by different techniques to better understand the cobalt species' nature. First, X-ray fluorescence spectroscopy was used to determine the cobalt loading of materials ($\text{CoN}_x@NC$ 1.3 % Co, $\text{Co}_2\text{P}@C$ 1.4 % Co, $\text{Co}_2\text{PN}_x@NC$ 1.8 % Co and $\text{Co}@C$ 1.6 % Co). High-angle annular dark-field scanning transmission electron microscopy (HAADF-STEM), high-resolution transmission electron microscopy (HRTEM), and energy-dispersive X-ray spectroscopy (EDX) investigations were conducted to explore the structural differences between the catalysts (Fig. 1).

Fig. 1 illustrates representative HAADF-STEM images of all catalysts. It can be seen that $\text{Co}_2\text{P}@C$ and $\text{Co}_2\text{PN}_x@NC$ catalysts present a significant fraction of nanoparticles with a rectangular prism shape in the size range of 20–40 nm (Fig. 1b, c). For these catalysts, close-up HRTEM images of one single nanocrystal show lattice fringes with d spacings of 2.2 Å, which may be ascribed to the (112) plane of the Co_2P (Fig. 1f, g) (JCPDS: 01–089-3030). As also observed in Fig. 1c, the particles show two distinct, rounded, and elongated morphologies. STEM-XEDS analysis of $\text{Co}_2\text{PN}_x@NC$ indicated that, in both types of nanoparticles, Co and P are mixed at the atomic level (Figure S1) in a phosphide-type phase. The intensity line profiles across the section of this nanostructure evidenced compositional differences in the core-shell structure observed in the HAADF-STEM image. In fact, P is concentrated within the core areas, where the overall Co:P molar ratio amounts to roughly 2:1 in both examples (Figure S1e, j). The shell is composed mainly of Co and O, in a ratio of about 1:2.5, indicating oxidation of the inner, phosphide-type core. Therefore, these results strongly support the formation of Co_2P nanocrystals in the P-containing catalysts (Table S1). An examination at high magnification of the support,

Figure S2a, confirms that a small fraction of cobalt is present as species dispersed at the atomic level, as metal clusters. The XEDS analysis on those areas, Figure S2b, clearly shows the Co-K signals and the quantification of the Co content, in the form of ultra-highly dispersed species, is roughly 0.1–0.15 %. In addition, the presence of N in these areas was confirmed by XEDS analysis (Figure S2b).

The HAADF-STEM images of the $\text{Co}@C$ catalyst (Fig. 1d and l) show nanoparticles around 20 nm in size with a core-shell structure. Two different interplanar distances can be observed in the HRTEM image: 2.5 and 1.5 Å, which match with CoO (JCPDS: 00–048-1719) and metallic Co (JCPDS of Co: 00–015-0806), respectively (Fig. 1h). The detailed XEDS analyses of representative Co nanoparticles, Figure S3, reveal the presence of an oxide layer, 10–12 nm thick, covering its surface, Figure S3c–f.

Finally, $\text{CoN}_x@NC$ exhibits a large area without any noticeable Co particles supported on the matrix (Fig. 1a) besides sporadic 20 nm Co particles. Fig. 2 gathers the most relevant results of an aberration-corrected HAADF-STEM study of the $\text{CoN}_x@NC$ catalyst. Co is present mainly in the form of an ultra-dispersed phase consisting of sub-nanometer clusters. Since the contrast in HAADF-STEM images depends roughly on the Z^2 values in the imaged area and the atomic number of Co ($Z = 27$) is much larger than those of C ($Z = 6$) or N ($Z = 7$), the Co-containing species appear as brighter areas in these images. Moreover, in the case of the highly dispersed species, the corresponding Co-K peaks could be detected in the XEDS spectra, Fig. 2d, also evidencing the presence of N in the XEDS and EELS spectra (Fig. 2d–e, Fig. S4).

The XRD patterns of the as-synthesized Co-based catalysts shown in Figure S5 are consistent with the formation of different species. The analysis of the patterns reveals that, besides the broad contribution

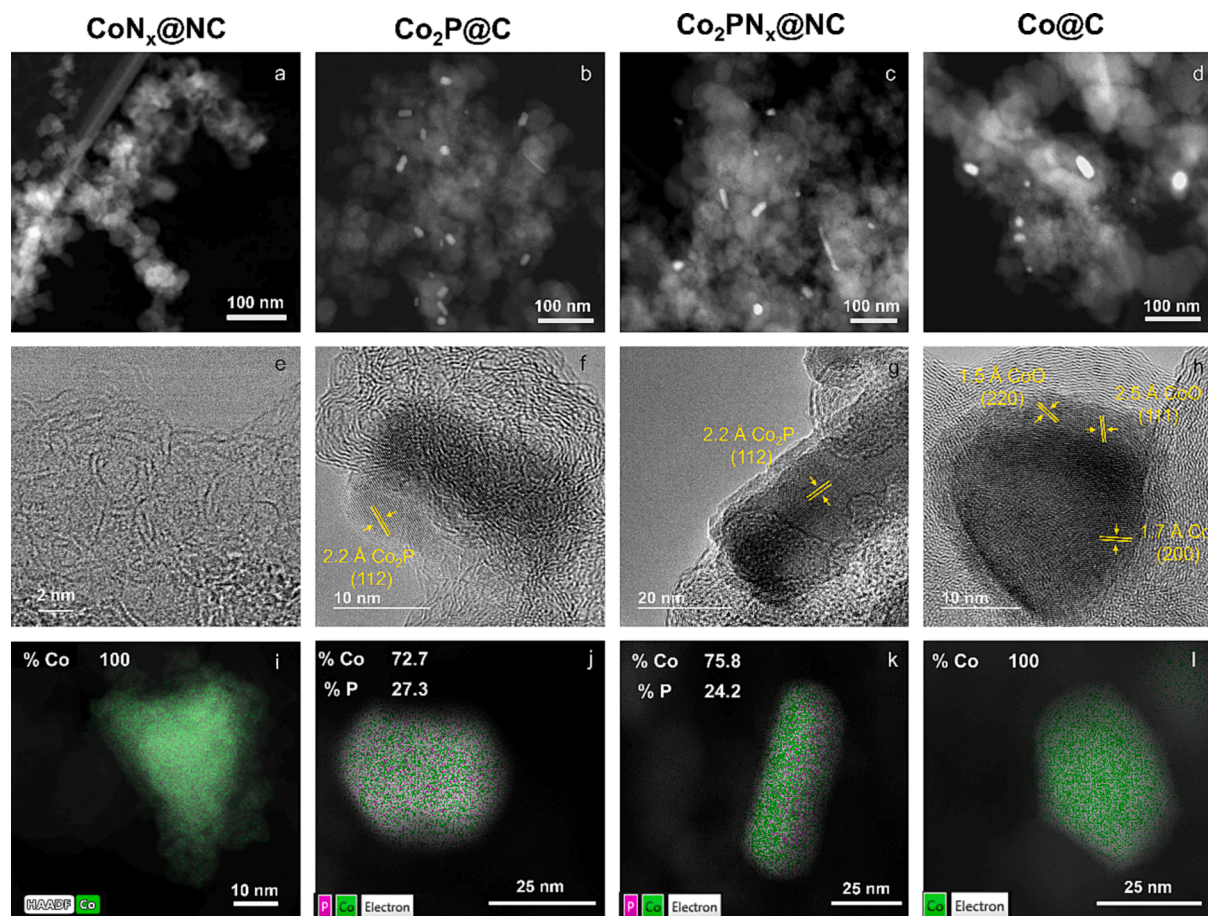


Fig. 1. HAADF-STEM images of a) $\text{CoN}_x@NC$, b) $\text{Co}_2\text{P}@C$, c) $\text{Co}_2\text{PN}_x@NC$, and d) $\text{Co}@C$. HRTEM images of e) $\text{CoN}_x@NC$, f) $\text{Co}_2\text{P}@C$, g) $\text{Co}_2\text{PN}_x@NC$ and h) $\text{Co}@C$. HAADF-STEM image and elemental mapping with EDX of i) $\text{CoN}_x@NC$, j) $\text{Co}_2\text{P}@C$, k) $\text{Co}_2\text{PN}_x@NC$, and l) $\text{Co}@C$.

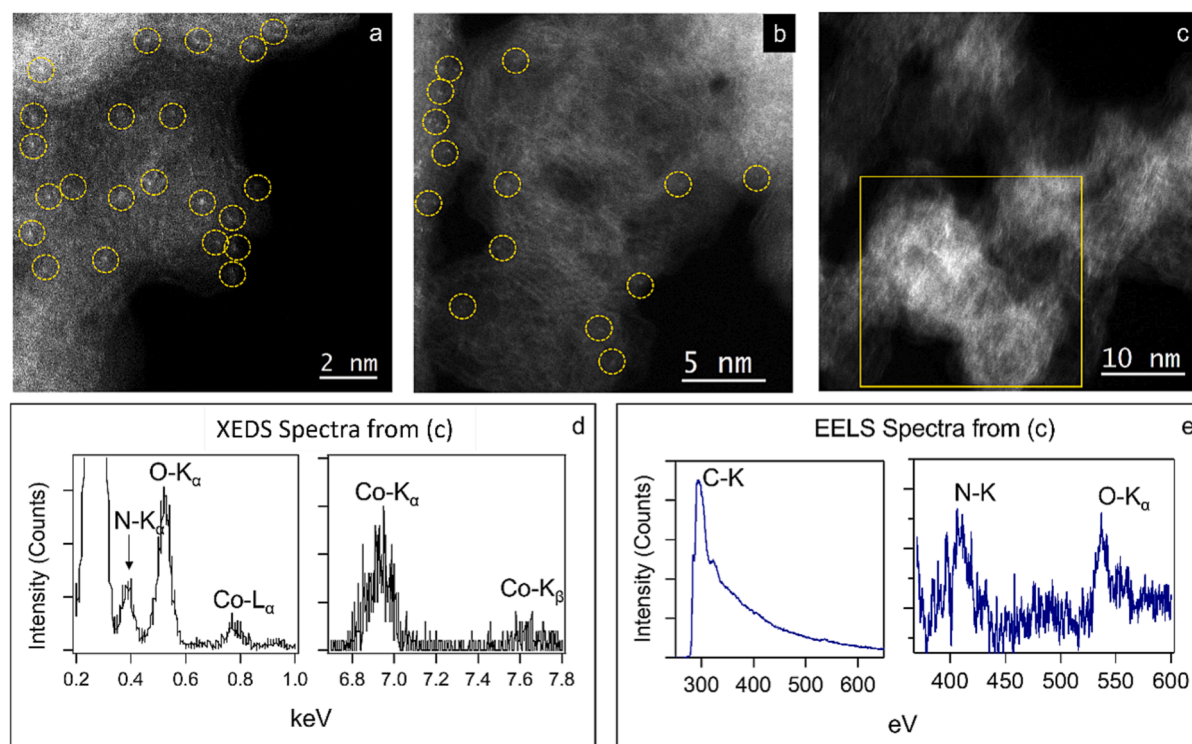


Fig. 2. a-c) High Resolution HAADF-STEM images of areas showing ultradispersed Co species in $\text{CoN}_x@NC$. d) XEDS and e) EELS spectra were taken from the inset at c), showing the typical signals found in this sample (Nitrogen, Cobalt, Oxygen, and Carbon).

attributed to the carbon-based support, $\text{CoN}_x@NC$ contains mainly metallic Co, while $\text{Co}_2\text{P}@C$ and $\text{Co}_2\text{PN}_x@NC$ primarily consist of Co_2P , in good agreement with HRTEM and STEM observations (See SI).

X-ray absorption spectroscopy was used to study the local environment and the electronic properties of Co-based materials. Fig. 3a shows the XANES spectra at the Co K-edge of the samples. The spectra of $\text{CoN}_x@NC$ and $\text{Co}@C$ present similar features to those of the Co foil but with a higher whiteline intensity, indicating some degree of metal oxidation. This oxidation can be further observed from the low-R contribution characteristic of Co-L (L = C, N, O) bonds at the Fourier Transform (FT) of these catalysts (Fig. 3b). Notwithstanding, the XANES of these two catalysts show flattened oscillations beyond the edge, pointing out a reduction in nanoparticle size with respect to the Co bulk (discussed later in the EXAFS part). As expected, the $\text{Co}_2\text{P}@C$ sample exhibits the same XANES features as the bulk Co_2P .

However, as for the samples with metallic features, the whiteline of the $\text{Co}_2\text{P}@C$ spectrum is higher in intensity than its standard counterpart, suggesting further oxidation. Lastly, the $\text{Co}_2\text{PN}_x@NC$ spectrum presents features of both metallic and Co_2P phases, with oscillations beyond the edge encompassing the two phases. The moduli of FT of the samples are represented in Fig. 3b, with the inset showing the EXAFS signal in k-space. The reduction in particle size for the Co^0 -containing samples can be observed by a significant decrease in the intensity of the Co-Co contribution at $\sim 2.19 \text{ \AA}$ ($\text{CN}_{\text{Co-Co}} = 5.4$, Table S2). $\text{Co}_2\text{P}@C$ displays a first shell split between the Co-P and Co-Co bonds with lower intensity than the bulk counterpart, pointing to a nanoscaled cobalt phosphide phase. The most complex sample, composed of Co_2P and Co^0 phases ($\text{Co}_2\text{PN}_x@NC$), presents mixed contributions from the two crystalline phases, which can be better observed in the inset of Fig. 3b. Its features with higher k-values overlap with those of the Co foil, while those at lower k-values start to overlap with bulk Co_2P . The distances obtained from EXAFS fittings for Co^0 - and Co_2P -based are in good agreement with those obtained by TEM with reported literature of similar systems [27,31].

The Continuous Cauchy Wavelet-Transforms (CCWT) presented in Fig. 3(c-f) can further support the previous discussion. In the Co^0 -rich

catalysts, $\text{CoN}_x@NC$ and $\text{Co}@C$, a main scattering lobe (red circle between 2.0 and 2.5 \AA of Y-axis) related to Co-Co distance was seen beside a faint Co-L blue scattering lobe between 1 and 2 (Y-axis). The $\text{Co}_2\text{P}@C$ catalyst displays the same contour plot as its reference counterpart, as shown in Figure S6. Notwithstanding, the $\text{Co}_2\text{PN}_x@NC$ system contains a mixture of scattering signals from Co^0 and Co_2P , with the red Co-Co scattering lobe shifted to higher k-values and much less intense Co-P scattering lobe than $\text{Co}_2\text{P}@C$, endorsing the coordination numbers obtained by EXAFS fitting. Overall, these results suggest that phosphorus is intercalated in the metallic structure as Co_2P while N is on the Co surface. In this context, NAP-XPS quantification (Table S3) reinforces this conclusion.

2.3. Catalytic activity

The catalysts prepared in this work were evaluated in the hydroformylation reaction of 1-hexene as a substrate to study the effect of N and P on Co-based catalysts (Table 1). Conversions and yields vary considerably between catalysts, which are also affected by a reduction treatment before testing. $\text{Co}@C$ did not show any catalytic activity for 20 h without the in-situ reduction (Table 1, entry 5) as opposed to the 77 % conversion of $\text{CoN}_x@NC$ (Table 1, entry 2). However, reduction of $\text{Co}@C$ for 2 h removed the cobalt oxide layer around the particle and achieved complete conversion with excellent selectivity to aldehydes (Table 1, entry 6). Such reducing treatment was not a requirement of $\text{CoN}_x@NC$ to obtain high conversions with good chemoselectivity towards the aldehydes and regioselectivity towards the linear aldehyde (Table 1, entry 3). In addition, a conversion of 94 % and 80 % of selectivity towards aldehydes was achieved with this catalyst in only 7.5 h by increasing the temperature to 120 $^\circ\text{C}$. In this regard, hexane from the reduction process is not observed, and the isomerization products of 1-hexene are minimized, which improves the ratio of linear aldehydes. The difference between these two samples proves that the incorporation of N brings crucial protection against oxidation and eliminates the necessity for a reducing step during catalyst activation.

On the other hand, the catalytic activity of $\text{Co}_2\text{P}@C$ was drastically

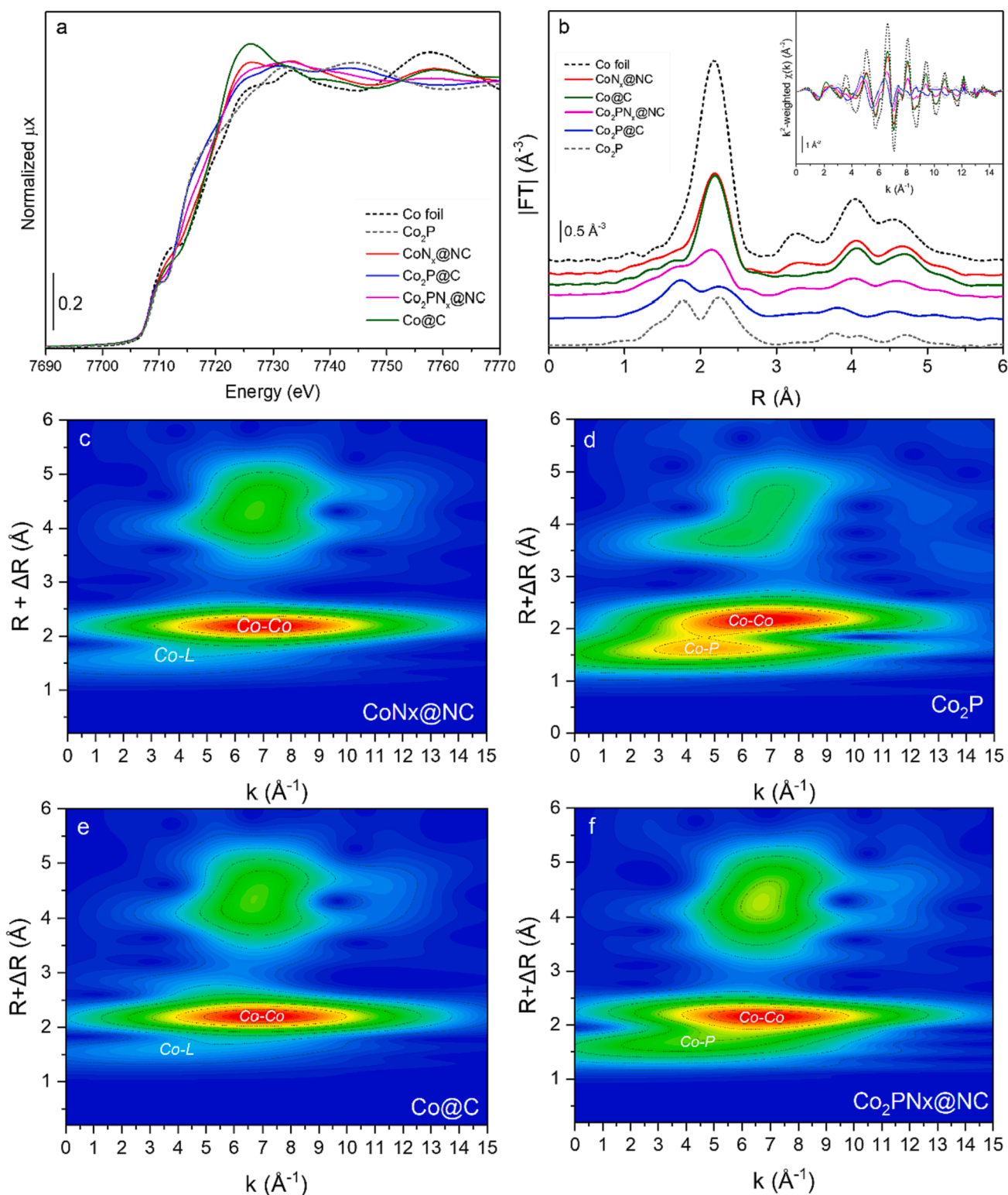


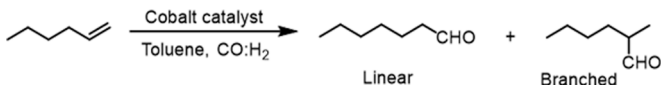
Fig. 3. a) XANES spectra at Co K-edge, b) k^2 -weighted, no phase corrected, $|FT|$ of Co-based samples and standards, (c-f) Continuous Cauchy Wavelet-Transforms of the EXAFS signal of Co-based catalysts.

reduced compared to $\text{Co}@C$ and $\text{CoN}_x@C$, even when the reduction treatment was applied (Table 1, entries 9, 10). The material with N-doped carbon coating around Co_2P particles ($\text{Co}_2\text{PN}_x@NC$) showed lower conversions than $\text{CoN}_x@NC$ but the same trends upon the mentioned reduction treatment (Table 1, entries 9, 10). Compared with Rh_2P -based catalysts, incorporating phosphorus within the particle does not boost the Co catalytic performance [30]. The partially positive

charge on Co and the partially negative charge on P, linked to an electron transfer from Co to P, are not beneficial for the reaction development. Nonetheless, these first catalytic tests proved how a N-doped carbon layer around the particle protects it against further oxidation, streamlining the overall process.

H/D exchange tests at different temperatures (25, 60, 90, and 120 °C) were used to study the impact of nitrogen and phosphorus on H_2

Table 1
Hydroformylation of 1-hexene on cobalt catalysts ^a.



Entry	Catalyst	Pretreat.	Conversion (%)	Aldehyde (%)	Aldehyde l:b	Alkane (%)	Isomerization (%)
1	[Co(tpy) ₂](NO ₃) ₂	–	0	–	–	–	–
2	CoN _x @NC	–	77	85	3.3:1	–	15
3	CoN _x @NC	H ₂ , 200 °C, 2 h	88	75	2.4:1	–	25
4	CoN _x @NC ^b	–	94	80	1.8:1	–	20
5	Co@C	–	0	–	–	–	–
6	Co@C	H ₂ , 200 °C, 2 h	95	99.5	3.5:1	–	0.5
7	Co ₂ P@C	–	3	100	0.6:1	–	–
8	Co ₂ P@C	H ₂ , 200 °C, 2 h	43	88	3.2:1	–	12
9	Co ₂ PN _x @NC	–	30	80	3.3:1	–	20
10	Co ₂ PN _x @NC	H ₂ , 200 °C, 2 h	32	94	3.8:1	–	6

^a Reaction conditions: cobalt catalyst at 1 wt%, Co:C₆H₁₂ ratio 1:300, 1-hexene 1.5 mmol, 100 °C, *p* = 40 bar CO:H₂ (1:1), 1.5 mL toluene, 20 h.

^b Reaction conditions: cobalt catalyst at 1 wt%, Co:C₆H₁₂ ratio 1:300, 1-hexene 1.5 mmol, 120 °C, *p* = 40 bar CO:H₂ (1:1), 1.5 mL toluene, 7.5 h.

dissociation efficiency. Consistently, CoN_x@NC exhibited the fastest H₂ dissociation, followed by Co₂PN_x@NC, Co₂P@C, and Co@C. This trend was confirmed by the evolution of HD/H₂ ratios during the experiments (Figure S7). The higher HD formation rate in CoN_x@NC may explain its superior catalytic activity in hydroformylation reactions. Additionally, kinetic analyses at different temperatures (100, 120, and 140 °C) were carried out with the CoN_x@NC catalyst (Figure S8). An excellent aldehyde selectivity (>85 %) was found at 100 °C. An even more rapid 1-hexene conversion (94 %) with high aldehyde selectivity (80 %) occurred in 7.5 h at 120 °C. Finally, at 140 °C, the conversion took only 3 h but with reduced aldehyde selectivity (58 %). The analysis provided an activation energy of 89.4 kJ/mol (Figure S8d). Other substrates besides 1-hexene were employed with CoN_x@NC as catalyst to determine activity limitations in some cases (Table S4).

2.4. Operando studies on the catalytic system: Near ambient pressure XPS

Operando X-ray photoelectron spectroscopy was employed to investigate the surface chemical state of the catalysts, both as-synthesized and under conditions resembling those of the reaction (Fig. 4 and Fig. S9). The C 1s spectra of the four prepared catalysts (Fig. 4d) are similar; they present three components with maxima at ca. 284.5, 285.3 and 286.2 eV. These contributions can be attributed to graphitic, aliphatic (-CH_x), and oxidized carbon species (carbon atoms with -C-N, and -CHOH or -COH groups, respectively) [32]. Regarding the Co 2p core level spectra, Co oxide and Co-N species present close binding energies values which makes determination of oxidation state challenging.

The Co 2p_{3/2} signal (Fig. 4a) reflects two broad peaks at ca. 780.5 ± 0.2 eV and 786.0 ± 0.2 eV associated with the main feature and satellite signal of Co^{δ+}, what could correspond to Co^{δ+}-O, Co^{δ+}-N or Co^{δ+}-P species in the studied catalysts [33,34]. It is worth noting that the peak of the Co@C sample presents a slightly different shape, including an additional feature at ca. 779.5 eV, typically associated with Co³⁺, which may indicate the presence of Co₃O₄ on the surface of the particles [35]. In addition, a narrower feature (FMWH 1.1 eV) is clearly observed at lower binding energies in the heteroatom-doped samples with maxima at ca. 778.5 ± 0.1 eV. This feature could be associated with metallic Co, but also be consistent with the presence of Co cobalt phosphide in the P-doped samples [26,31,33,34,36,37]. The N 1s spectra (Fig. 4b) presented contributions at ca. 398.8 and 400.2 eV, respectively, attributed to pyridinic nitrogen and N-Co species [33,38]. A similar situation has been observed in the P 2p spectra (Fig. 4c), where two 2p_{3/2} and 2p_{1/2} doublets with P 2p_{3/2} values at ca. 129.6 and 133.3 eV are observed, that are assigned to P as phosphide and as phosphate, respectively [31,37,39].

The NAP XPS spectra confirmed the presence of C-N patches on CoN_x@NC and Co₂PN_x@NC samples, while the Co₂P@C and Co₂PN_x@NC spectra also support the presence of the Co₂P phase. Interestingly, the Co is partially reduced on N-containing samples, which aligns with the inhibition of Co atoms' leaching and the enhancement of the activity seen for the as-synthesized samples.

2.5. Stability and heterogeneity Co-based catalysts

It is crucial to study the stability of the material during the catalyst development for hydroformylation. In the present section, the leaching of the active phase was investigated to reveal suppression of metal loss when introducing the heteroatom. At this stage, the difference in leached Co between CoN_x@NC (Table 2, entries 1, 2) and Co@C is tentatively ascribed to the N-doped graphitic carbon layers over Co nanoclusters in CoN_x@NC. These layers are supposed to anchor the Co species and avoiding a strong Co interaction to carbon monoxide as in bare NPs in Co@C (Table 2, entry 3), mitigating the formation of soluble cobalt carbonyl species. This last statement has been corroborated through CO and H₂ chemisorption studies over CoN_x@NC [27]. For this catalyst, chemisorption did not occur, which supports that this synthesis methodology promotes metal centers which are less accessible. H₂ chemisorption experiments were also performed on Co₂P-based catalysts and on the unmodified Co@C catalyst (Table S5). These results reveal the higher accessibility of metal centres for the uncovered Co nanoparticles in Co@C as opposed to the ones in Co₂PN_x@NC and Co₂P@C. This, in turn, indicates the higher coverage and protection of the N-doped carbon layer in Co₂PN_x@NC first, and in Co₂P@C, secondly, in comparison to Co@C.

Metal leaching was also reduced for Co₂P@C and Co₂PN_x@NC catalysts (Table 2, entries 4, 5). In the case of Co₂PN_x@NC, the reason is the presence of an N-doped carbon layer like in CoN_x@NC, and in Co₂P@C, it is likely due to a non-nitrogenated carbon covering. However, the greater leaching observed in this sample (6.2 %) reinforces the positive role of nitrogen in anchoring cobalt. Remarkably, all catalysts prepared with a stabilizing ligand, either nitrogen or phosphorus-based, have successfully reduced cobalt leaching, demonstrating the efficient protection of carbon layers. Table 2 (entries 6–9) provides a crucial comparison with the leaching results of other cobalt catalysts [19–22]. Notably, when evaluating Turnover Numbers (TON) and productivity, CoN_x@NC stands out with markedly higher values than the best-performing heterogeneous cobalt catalyst reported in the literature [19–22]. Impressively, this superior performance holds even when the reaction temperature is lower by at least 30 °C, underscoring the notable efficiency of CoN_x@NC in the hydroformylation process.

As one of the most active and resilient solid catalysts ever tested, the

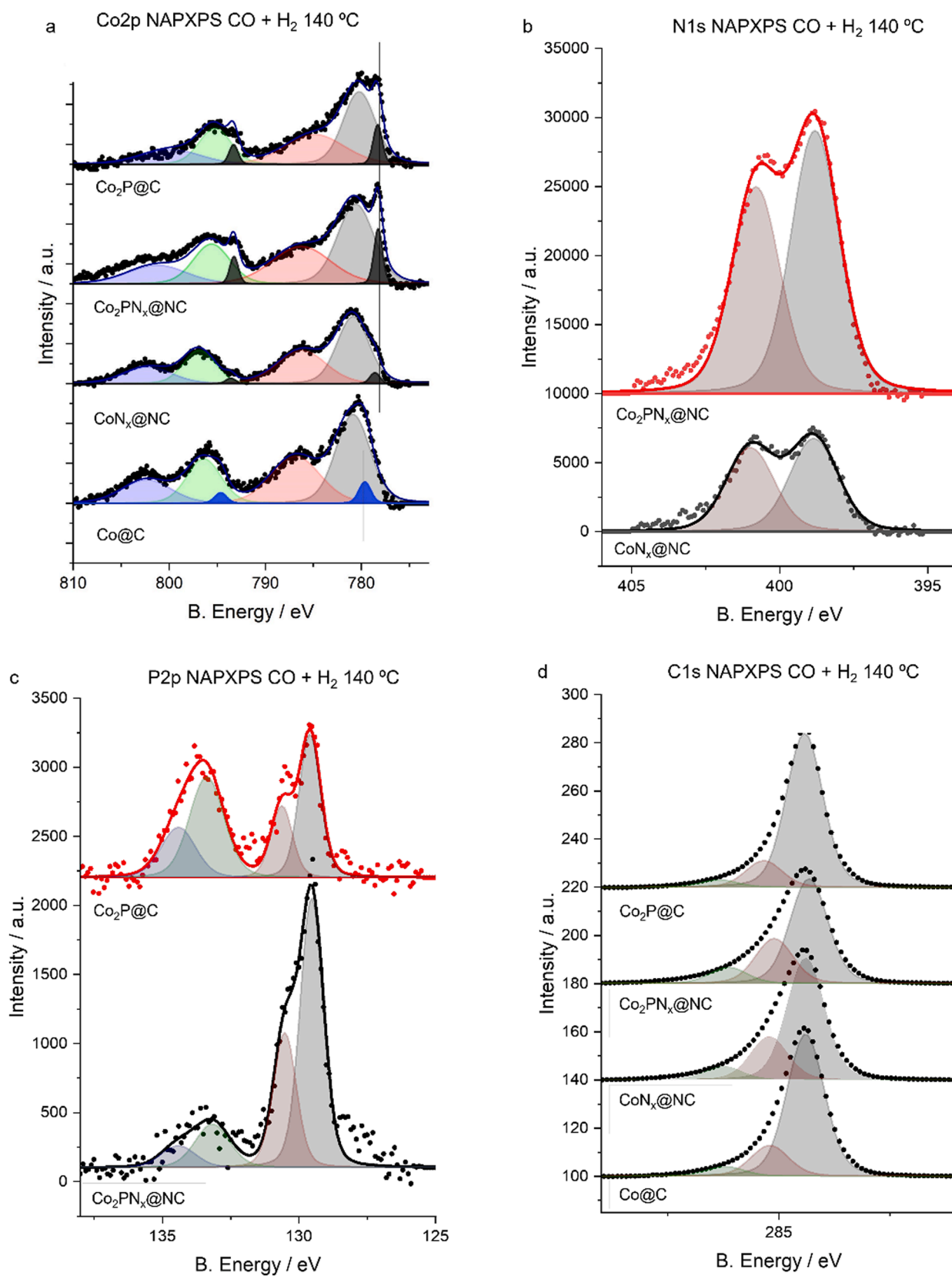


Fig. 4. NAPXPS spectra of a) Co 2p line, b) N 1 s line, c) P 2p line, and d) C 1 s line under reaction conditions.

Table 2

Turnover Numbers (TONs), productivities per mol of Co, and quantities of leached Co for the catalysts synthesized in this study and those reported in the literature ^a.

Entry	Catalyst	TON ^b	mol prod·mol Co ⁻¹ ·h ⁻¹	T (°C)	% Leached Co ^c
1	CoN _x @NC	218.1	7.6	100	1.9
2	CoN _x @NC ^d	221.0	7.7	100	0.3
3	Co@C	281.4	8.8	100	48.6
4	Co ₂ P@C	126.7	4.0	100	6.2
5	Co ₂ PN _x @NC	94.3	2.5	100	0.7
6	Co/phen@C ^e	46.5	3.9	100	23
7	Co/SiO ₂ ^f	30.3	1.7	100	0.2
8	CoZrP-2.0 ^g	13.6	2.1	160	0.5
9	CoGaSiO ₂ ^h	27.5	4.5	130	1.7

^a Reaction conditions: cobalt catalyst at 1 wt% (0.0051 mmol Co), Co:C₆H₁₂ ratio 1:300, olefin 1.5 mmol, *p* = 40 bar CO:H₂ (1:1), 100 °C, 1.5 mL toluene, 20 h.

^b TONs were calculated with the number of mmol of converted reactant, and total mmol of Co.

^c Leached Co amounts were obtained by ICP-MS analyses.

^d After four runs of use.

^e From the work of Beller et al. [19].

^f From the work of Wen et al. [20] From the work of Hou et al. [21] From the work of Wen et al. [22].

CoN_x@NC sample underwent a thorough examination of its stability and heterogeneity. Remarkably, the CoN_x@NC catalyst sustained its activity and selectivity through a minimum of four reuses, as evident in Fig. 5a. Notably, the level of Co leaching approached zero (0.3 %) after the fourth cycle, underscoring the exceptional durability and resilience of the catalyst. Additionally, a hot filtration test confirmed its heterogeneity. Upon filtration and retesting, no further increase in the 1-hexene conversion was observed, demonstrating its outstanding stability and its role as a genuine heterogeneous catalyst (Fig. 5b).

2.6. Atomistic modelling of CoN_x@NC

The various characterization techniques employed on CoN_x@NC samples showed the presence of small Co clusters (Fig. 2) with low coordination numbers (Table S2) and binding nitrogen atoms (Fig. 3). These clusters proved to be very active in the hydroformylation of 1-hexene and remarkably resistant to metal leaching (Table 2). We used computational simulations (see section 2 in the SI) to understand the effect of N binding and Co atoms' coordination on the cohesive interaction between Co atoms in the clusters as a measure of the resistance to leach. The Co cluster was placed in direct contact with four different models of protective carbon patches (Fig. 6 a–d).

For each cluster (Co_n), the cohesion energies of at least five different atoms (Co₁) showing the lowest coordination were independently evaluated using Equation (1) (Figure S15). The coordination was measured using 1.2 times the radius of the atoms involved [40]. Once the weakest cohesion was identified, the Co_{n-1} cluster was relaxed to proceed with another leaching step, providing insight into the cluster's size effect against leaching.

$$E_{Coh} = E_{Co_{n-1}/Support} + E_{Co_1} - E_{Co_n/Support} \quad (1)$$

The almost 400 structures examined led to common outcomes independent of the support. (i) The surface atoms in Co_n with *n* ≥ 6 have coordination between 4 and 6 (Figure S10). (ii) The average interatomic distance between the examined atoms and their neighbours is close to the bulk's Co-Co distance in Co_n with *n* ≥ 10 and decreases with cluster size. The results on the support with one pyridinic nitrogen are more dispersed than on SV, gN, and 3pN (Figure S11). The average Co-Co distance showed a relationship with the atom's coordination, although it is not an accurate descriptor as it depends on unidentified variables (Figure S13). (iii) The atomic cohesion energy is generally lower than the bulk one, 4.85 eV/atom (Figure S12) [41,42]. However, it is much higher in the Co atoms close to the support's atoms; note that gN does not present dangling bonds. Contrarily to the average interatomic distance, the atomic coordination number seems a suitable descriptor for the cohesion energy, a measure against leaching, when considering the effect of the support's dangling bonds (Figure S14).

Fig. 6 (e–h) shows the values of the atoms more prompt to leaching, their coordination in the Co_n cluster, and the average Co-Co distance from its neighbors. The first observation is that *E*_{coh} and interatomic distances are interdependent; both parameters increase with the cluster size, especially in the presence of surface N atoms. There are two critical outcomes: Co atoms with the lowest coordination leach easier than highly coordinated ones, and Co atoms interacting with the surface significantly stabilize them and mitigate leaching. Both statements align with the experimental observations and explain the resilience of the small particles on the CoN_x@NC sample before and after the aggressive hydroformylation reaction.

3. Conclusions

This work presents alternative methods to suppress cobalt metal leaching during hydroformylation conditions in liquid phase without involving additives, which is the main challenge for this process. Ligands containing N and P have been used as dopant sources to form protective carbon patches around Co particles, the active phase. These coatings have proven to be highly effective in preserving the supported nanoparticles during and after the hydroformylation in liquid phase. Moreover, N and P ligands served as dopant precursors to originate CoN_x and

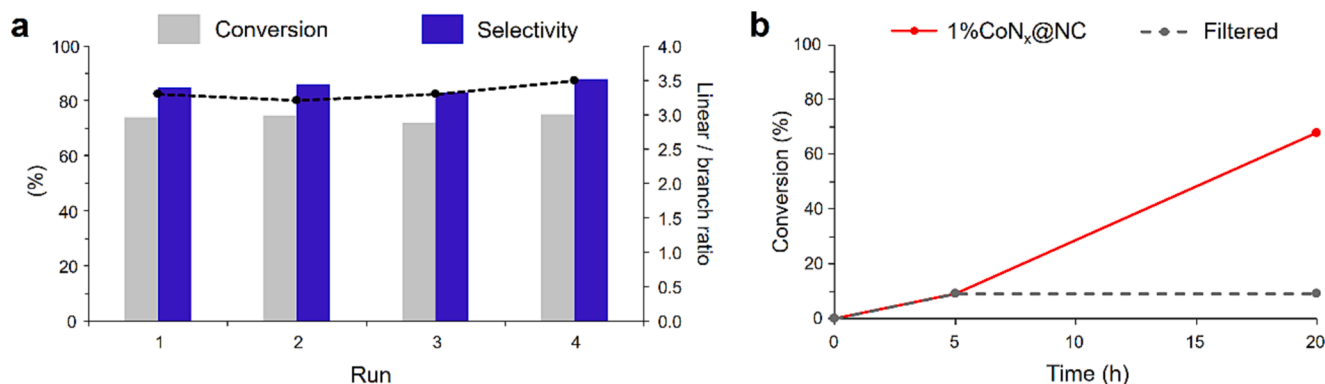


Fig. 5. A) conversion (grey), selectivity to aldehydes (blue), and linear to branched ratio (black dashed line) for four reaction runs with CoN_x@NC as a catalyst. B) Reaction profiles for experiments performed with CoN_x@NC as catalyst (red line) and after hot filtration (grey dotted line). (For interpretation of the references to colour in this figure legend, the reader is referred to the web version of this article.)

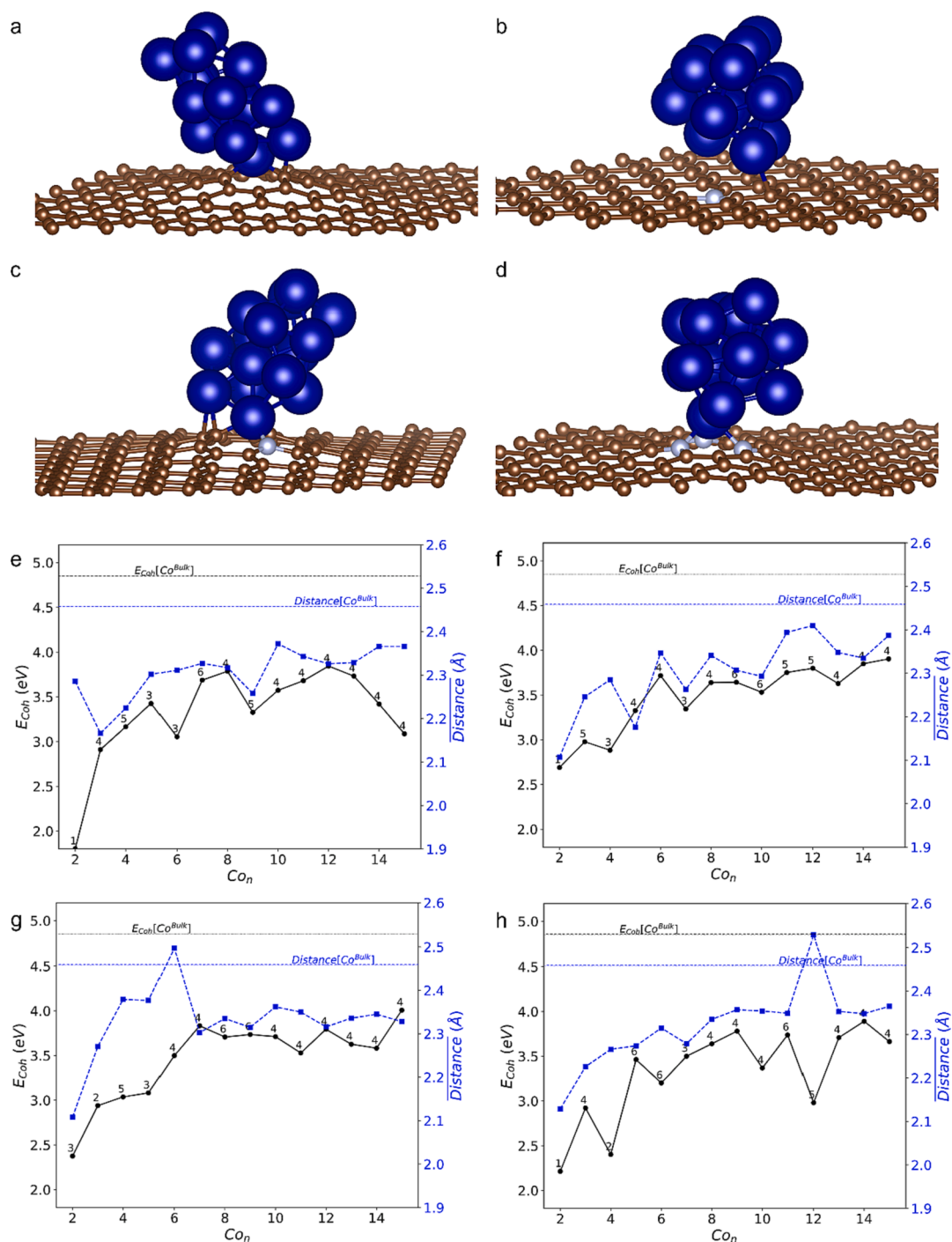


Fig. 6. (a-d) Schematic representation of tendencies of the cohesion energy and Co-Co distance for the optimized Co₁₅ cluster on a) single C-vacancy graphene, b) graphitic N-doped graphene, c) pyridinic N-doped graphene, and d) graphene doped with three pyridinic N atoms. The colour scheme is brown, light blue, and deep blue for C, N, and Co atoms and bonds. (e-h) Cohesion energies (E_{Coh}) and average interatomic distances (Distance) of the atoms more prompt to leach as a function of the cluster's size (n) on e) single C-vacancy graphene, f) graphitic N-doped graphene, g) pyridinic N-doped graphene, and h) graphene doped with three pyridinic N atoms. Horizontal lines indicate the Co bulk values. (For interpretation of the references to colour in this figure legend, the reader is referred to the web version of this article.)

Co₂P nanoparticles, respectively. While the introduction of P resulted in particles with a Co-P core, offering enhanced leaching resistance but no improvement in catalytic performance, the utilization of N-containing ligands resulted in materials where the presence of N in the patches emerged as a pivotal factor. This configuration in the CoN_x@NC material exhibited outstanding catalytic activity, coupled with remarkable resistance to cobalt oxidation and leaching. Notably, this work represents one of the best-reported results for a heterogeneous catalyst in

liquid-phase hydroformylation, achieving an exceptional balance between stability and activity.

CRedit authorship contribution statement

Carmen Galdeano-Ruano: Writing – original draft, Methodology, Investigation. **Silvia Gutiérrez-Tarriño:** Writing – review & editing, Writing – original draft, Methodology, Investigation, Formal analysis.

Christian W. Lopes: Writing – original draft, Investigation, Formal analysis. **Jaime Mazarío:** Writing – review & editing, Writing – original draft, Methodology. **Lidia E. Chinchilla:** Methodology. **Giovanni Agostini:** Writing – original draft, Formal analysis. **Jose J. Calvino:** Writing – review & editing, Writing – original draft, Investigation. **Juan P. Holgado:** Writing – original draft, Formal analysis. **Enrique Rodríguez-Castellón:** Writing – review & editing. **Alberto Roldan:** Writing – review & editing, Writing – original draft, Methodology, Investigation, Formal analysis, Data curation. **Pascual Oña-Burgos:** Writing – review & editing, Writing – original draft, Supervision, Funding acquisition, Conceptualization.

Declaration of competing interest

The authors declare that they have no known competing financial interests or personal relationships that could have appeared to influence the work reported in this paper.

Data availability

Data will be made available on request.

Acknowledgments

The authors thank the financial support from the Spanish Government (RTI2018-096399-A-I00, PID2022-140111OB-I00, PID2020-113006-RB-I00, TED2021-130191B-C41, TED2021-130756B-C31 and TED2021-130191B-C44, PID2020-119946RB-I00, US-1263455 funded by MCIN/AEI/ 10.13039/501100011033 and European Union Next-GenerationEU/PRTR). This project has received funding from the European Union's Horizon 2020 research and innovation programme under grant agreement No 101022507. HR-STEM studies were performed at the DME-UCA node of the ELECMI Spanish Unique Infrastructure (ICTS) for Electron Microscopy of Materials. We also acknowledge the supercomputing Wales for access to the Hawk HPC facility, part-funded by the European Regional Development Fund via the Welsh Government. Some of these experiments were performed at CLAES (beamtime 2021095439) and CIRCE (beamtime 2022096991) beamlines at ALBA Synchrotron with the collaboration of ALBA staff (Virginia Pérez, Ignacio Villar and Carlo Marini).

Appendix A. Supplementary data

Supplementary data to this article can be found online at <https://doi.org/10.1016/j.jcat.2024.115374>.

References

- R. Franke, D. Selent, A. Börner, Applied hydroformylation, *Chem. Rev.* 112 (2012) 5675–5732.
- J. Pospech, I. Fleischer, R. Franke, S. Buchholz, M. Beller, Alternative metals for homogeneous catalyzed hydroformylation reactions, *Angew. Chemie - Int. Ed.* 52 (2013) 2852–2872.
- F.M.S. Rodrigues, R.M.B. Carrilho, M.M. Pereira, Reusable catalysts for hydroformylation-based reactions, *Eur. J. Inorg. Chem.* (2021) 2294–2324.
- B. Wang, J.F. Chen, Y. Zhang, Synthesis of highly dispersed cobalt catalyst for hydroformylation of 1-hexene, *RSC Adv.* 5 (2015) 22300–22304.
- C. Bauder, D. Sémeril, Styrene Hydroformylation with Cavity-Shaped Ligands, *Eur. J. Inorg. Chem.* (2019) 4951–4965.
- C. Li, W. Wang, L. Yan, Y. Ding, A mini review on strategies for heterogenization of rhodium-based hydroformylation catalysts, *Front. Chem. Sci. Eng.* 12 (2018) 113–123.
- F.G. Delolo, J. Yang, H. Neumann, E.N. Dos Santos, E.V. Gusevskaya, M. Beller, Cobalt-Catalyzed hydroformylation under mild conditions in the presence of phosphine oxides, *ACS Sustain. Chem. Eng.* 9 (2021) 5148–5154.
- N. Huang, B. Liu, X. Lan, T. Wang, Insights into the bimetallic effects of a RhCo catalyst for ethene hydroformylation: experimental and DFT investigations, *Ind. Eng. Chem. Res.* 59 (2020) 18771–18780.
- D.M. Hood, R.A. Johnson, A.E. Carpenter, J.M. Younker, D.J. Vinyard, G. D. Stanley, Highly active cationic cobalt(II) hydroformylation catalysts, *Science* (80-) 367 (2020) 542–548.
- F. Hebrard, P. Kalck, Cobalt-catalyzed hydroformylation of alkenes: generation and recycling of the carbonyl species, and catalytic cycle, *Chem. Rev.* 109 (2009) 4272–4282.
- Y. Zhang, K. Nagasaka, X. Qiu, N. Tsubaki, Hydroformylation of 1-hexene for oxygenate fuels on supported cobalt catalysts, *Catal. Today.* 104 (2005) 48–54.
- Y. Liu, Z. Li, B. Wang, Y. Zhang, A fine dispersed cobalt catalyst with macro-pore for hydroformylation of 1-hexene, *Catal. Letters.* 146 (2016) 2252–2260.
- W. Xu, Y. Ma, X. Wei, H. Gong, X. Zhao, Y. Qin, Q. Peng, Z. Hou, Core-shell Co@CoO catalysts for the hydroformylation of olefins, *New J. Chem.* 46 (2022) 15712–15722.
- Z. Cai, H. Wang, C. Xiao, M. Zhong, D. Ma, Y. Kou, Hydroformylation of 1-hexene over ultrafine cobalt nanoparticle catalysts, *J. Mol. Catal. A Chem.* 330 (2010) 94–98.
- M.C. Marcucci Ribeiro, (12) Patent Application Publication (10) Pub. No.: US 2004 / 0092606A1, United States - Pat. Appl. Publ. 1 (2004) 2002–2005.
- P. Shukla, H. Sun, S. Wang, H.M. Ang, M.O. Tade, Co-SBA-15 for heterogeneous oxidation of phenol with sulfate radical for wastewater treatment, *Catal. Today.* 175 (2011) 380–385.
- X. Huang, N. Zhu, X. Wei, Y. Ding, Y. Ke, P. Wu, Z. Liu, Mechanism insight into efficient peroxydisulfate activation by novel nano zero-valent iron anchored yCo3O4 (nZVI/yCo3O4) composites, *J. Hazard. Mater.* 400 (2020) 123157.
- B. Li, X. Li, K. Asami, K. Fujimoto, Low-pressure hydroformylation of middle olefins over Co and Rh supported on active carbon catalysts, *Energy Fuel* 17 (2003) 810–816.
- M.F. Hertrich, F.K. Scharnagl, A. Pews-Davtyan, C.R. Kreyenschulte, H. Lund, S. Bartling, R. Jackstell, M. Beller, Supported cobalt nanoparticles for hydroformylation reactions, *Chem. - A Eur. J.* 25 (2019) 5534–5538.
- J. Zhao, Y. He, F. Wang, W. Zheng, C. Huo, X. Liu, H. Jiao, Y. Yang, Y. Li, X. Wen, Suppressing metal leaching in a supported Co/SiO₂ catalyst with effective protectants in the hydroformylation reaction, *ACS Catal.* 10 (2020) 914–920.
- H. Gong, X. Zhao, Y. Qin, W. Xu, X. Wei, Q. Peng, Y. Ma, S. Dai, P. An, Z. Hou, Hydroformylation of olefins catalyzed by single-atom Co(II) sites in zirconium phosphate, *J. Catal.* 408 (2022) 245–260.
- J. Zhao, Y. He, F. Wang, Y. Yang, W. Zheng, C. Huo, H. Jiao, Y. Yang, Y. Li, X. Wen, A recyclable CoGa intermetallic compound catalyst for the hydroformylation reaction, *J. Catal.* 404 (2021) 244–249.
- W. Gao, S. Liu, Z. Wang, J. Peng, Y. Zhang, X. Yuan, X. Zhang, Outlook of Cobalt-Based Catalysts for Heterogeneous Hydroformylation of Olefins: From Nanostructures to Single Atoms, (2023).
- F.A. Westerhaus, R.V. Jagadeesh, G. Wienhöfer, M.M. Pohl, J. Radnik, A.E. Surkus, J. Rabeah, K. Junge, H. Junge, M. Nielsen, A. Brückner, M. Beller, Heterogenized cobalt oxide catalysts for nitroarene reduction by pyrolysis of molecularly defined complexes, *Nat. Chem.* 5 (2013) 537–543.
- S. Nandi, P. Patel, N.U.H. Khan, A.V. Biradar, R.I. Kureshy, Nitrogen-rich graphitic-carbon stabilized cobalt nanoparticles for chemoselective hydrogenation of nitroarenes at milder conditions, *Inorg. Chem. Front.* 5 (2018) 806–813.
- Y. Zhang, P. Cao, H.Y. Zhang, G. Yin, J. Zhao, Cobalt nanoparticles anchoring on nitrogen doped carbon with excellent performances for transfer hydrogenation of nitrocompounds to primary amines and N-substituted formamides with formic acid, *Catal. Commun.* 129 (2019) 105747.
- S. Gutiérrez-Tarriño, S. Rojas-Buzo, C.W. Lopes, G. Agostini, J.J. Calvino, A. Corma, P. Oña-Burgos, Cobalt nanoclusters coated with N-doped carbon for chemoselective nitroarene hydrogenation and tandem reactions in water, *Green Chem.* 23 (2021) 4490–4501.
- L.H. Slaugh, R.D. Mullineaux, Novel hydroformylation catalysts, *J. Organomet. Chem.* 13 (1968) 469–477.
- B. Liu, Y. Wang, N. Huang, X. Lan, T. Wang, Activity promotion of Rh₈-Co_xP₄ bimetallic phosphides in styrene hydroformylation: dual influence of adsorption and surface reaction, *ACS Catal.* 11 (2021) 9850–9859.
- C. Galdeano-Ruano, C.W. Lopes, D. Motta Meira, A. Corma, P. Oña-Burgos, Rh₂P nanoparticles stabilized by carbon patches for hydroformylation of olefins, *ACS Appl. Nano Mater.* 4 (2021) 10743–10753.
- Z. Chen, X. Zeng, X. Li, Z. Lv, J. Li, Y. Zhang, Strong metal phosphide-phosphate support interaction for enhanced non-noble metal catalysis, *Adv. Mater.* 34 (2022).
- G. Greczynski, L. Hultman, X-ray photoelectron spectroscopy: Towards reliable binding energy referencing, *Prog. Mater. Sci.* 107 (2020) 100591.
- C. Tang, A.E. Surkus, F. Chen, M.M. Pohl, G. Agostini, M. Schneider, H. Junge, M. Beller, A stable nanocobalt catalyst with highly dispersed Co_N active sites for the selective dehydrogenation of formic acid, *Angew. Chemie - Int. Ed.* 56 (2017) 16616–16620.
- W. Wu, L. Zong, X. Chen, W. Zhang, L. Cui, Y. Yang, X. Wang, S.X. Li, L. Wang, Co nanoislands activated Co, N-doped porous carbon nanospheres for highly efficient and durable oxygen electrocatalyst, *Appl. Surf. Sci.* 541 (2021) 148262.
- K.M. Cole, D.W. Kirk, S.J. Thorpe, Co₃O₄ nanoparticles characterized by XPS and UPS, *Surf. Sci. Spectra.* 28 (2021) 014001.
- G.R. Bhadu, B. Parmar, P. Patel, A. Paul, J.C. Chaudhari, D.N. Srivastava, E. Suresh, Co@N-doped carbon nanomaterial derived by simple pyrolysis of mixed-ligand MOF as an active and stable oxygen evolution electrocatalyst, *Appl. Surf. Sci.* 529 (2020) 147081.
- J.R. Hayes, R.H. Bowker, A.F. Gaudette, M.C. Smith, C.E. Moak, C.Y. Nam, T. K. Pratum, M.E. Bussell, Hydrodesulfurization properties of rhodium phosphide: comparison with rhodium metal and sulfide catalysts, *J. Catal.* 276 (2010) 249–258.
- V. García-López, N. Giaconi, L. Poggini, J. Calbo, A. Juhin, B. Cortigiani, J. Herrero-Martín, E. Ortí, M. Mannini, M. Clemente-León, E. Coronado, Spin-

- Crossover Grafted Monolayer of a Co(II) Terpyridine Derivative Functionalized with Carboxylic Acid Groups, *Adv. Funct. Mater.*, 2023.
- [39] K. Wang, B. Huang, F. Lin, F. Lv, M. Luo, P. Zhou, Q. Liu, W. Zhang, C. Yang, Y. Tang, Y. Yang, W. Wang, H. Wang, S. Guo, Wrinkled Rh₂P nanosheets as superior pH-universal electrocatalysts for hydrogen evolution catalysis, *Adv. Energy Mater.* 8 (2018) 1–7.
- [40] A. Hjorth Larsen, J. Jørgen Mortensen, J. Blomqvist, I.E. Castelli, R. Christensen, M. Dulak, J. Friis, M.N. Groves, B. Hammer, C. Hargus, E.D. Hermes, P.C. Jennings, P. Bjerre Jensen, J. Kermode, J.R. Kitchin, E. Leonhard Kolsbjerg, J. Kubal, K. Kaasbjerg, S. Lysgaard, J. Bergmann Maronsson, T. Maxson, T. Olsen, L. Pastewka, A. Peterson, C. Rostgaard, J. Schiøtz, O. Schütt, M. Strange, K. Thygesen, T. Vegge, L. Vilhelmsen, M. Walter, Z. Zeng, K.W. Jacobsen, The atomic simulation environment - a Python library for working with atoms, *J. Phys. Condens. Matter.* 29 (2017).
- [41] C. Kittel, *Introduction to solid state physics*, 2005.
- [42] E. Kaxiras, Applications of band theory, in: *At. Electron. Struct. Solids*, Cambridge University Press, 2003, pp. 160–202.